# Silicon-on-Insulator Slot-waveguide Design Trade-offs

Patrick Steglich[1,2], Claus Villringer[1], Silvio Dümecke[1], Yazmin Padilla Michel[1,2], Mauro Casalboni[2] and Sigurd Schrader[1]

[1]*Faculty of Engineering and Natural Sciences, University of Applied Sciences Wildau, Wildau, Germany*

[2]*Department of Industrial Engineering, University of Rome "Tor Vergata", Rome, Italy*

Keywords: Slot-waveguide, Silicon-organic Hybrid Technology, Optical Field Confinement, Effective Nonlinear Area.

Abstract: Silicon-on-insulator slot-waveguide structures are designed and analysed numerically. We present our theoretical investigation of field confinement factors and effective nonlinear areas for different waveguide structures in order to find optimized geometrical dimensions. It is shown that a slot-waveguide with a height of 220 nm, a slot width of 180 nm and a silicon rail width of 180 nm provides a five times higher field confinement in the cladding region compared to conventional strip-waveguides which explains the high sensitivity of slot-waveguide based label-free bio-sensors.



## 1 INTRODUCTION

The major advantage of slot-waveguides is the fact that the guided light is confined in-between two silicon rails (Almeida et al., 2004). Consequently, the light is forced to interact directly with the surrounding material. Figure 1 shows a detailed cross-sectional view and compares the guided optical field in a strip-waveguide to the one of a slot-waveguide. The reason for this high confinement in-between the silicon rails is the large-index contrast of the high-index silicon and the low-index surrounding material. At the interface the normal electric field, which is according to Figure 1 the $E_x$ field, undergoes a large discontinuity. This results in a field enhancement in the low-index region which is proportional to the ratio of the dielectric constant of the surrounding material to that of silicon.

The high confinement inside the slot is of special benefit for sensing and electro-optical applications. The so called silicon-organic hybrid (SOH) technology uses organic materials with exceptional high linear electro-optical coefficients as surrounding material (Vivien and Pavesi, 2013). Current electro-optic modulators are based on semiconductors like silicon. In silicon photonics, fundamental speed limitations are related to carrier injection and removal (Vivien and Pavesi, 2013). Therefore, parametric processes are impaired by nonparametric processes like two-photon absorption and become to the main speed limiting factor. Additionally, silicon has a lack of linear electro-optical coefficients. All this can be overcome by using organic materials with nonlinear optical properties as active material.

Slot-waveguides are the key element in order to integrate organic materials into silicon photonics. Because the organic materials offer high linear electro-optical coefficients once can generate advanced modulation formats (Korn et al., 2013). The reason for that is that organic materials have less free-carrier dispersion which normally leads to an intrinsic coupling of amplitude and phase. For that reason, slot-waveguides have been employed in order to develop high-speed modulators for telecommunication interconnects (Weimann et al., 2014).

In the last decade integrated optical sensors based on slot-waveguides have also been proposed (Dell'Olio and Passaro, 2007) and developed (Bar-

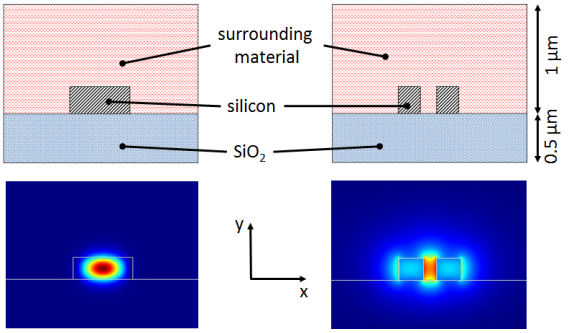


Figure 1: Cross-sectional view of a SOI strip-waveguide (left) and a SOI slot-waveguide (right). The pictures below show the optical field amplitude distribution. Both waveguide structures are on top of a buried oxide (BOX) substrate.

Steglich P., Villringer C., Dümecke S., Padilla Michel Y., Casalboni M. and Schrader S..
Silicon-on-Insulator Slot-waveguide Design Trade-offs.
DOI: 10.5220/0005336200470052
In *Proceedings of the 3rd International Conference on Photonics, Optics and Laser Technology* (PHOTOPTICS-2015), pages 47-52
ISBN: 978-989-758-093-2

rios et al., 2007). In case of label-free bio-sensors it has been shown that the sensitivity of slot-waveguides is more than three times higher compared to conventional silicon strip-waveguides (Claes et al., 2009). This fact is due to the high interaction between guided light and the surrounding material.
The most challenging issue of SOH technology based slot-waveguides is the compatibility with common complementary-metal-oxide-semiconductor (CMOS) fabrication processes since such integrated photonic devices need a high integration rate and a cost efficient mass production environment.
For that reason, in this work we present design tradeoffs and an approach in order to improve SOI slot-waveguide structures for a CMOS-like production environment. Typical figures of merit like the field confinement factor and the effective nonlinear area are calculated and discussed in detail.
There are several publications about field confinement factors of slot-waveguide structures. These structures consist of vertical silicon rails (Robinson et al., 2008) or multiple nanolayers (Feng et al., 2006). However, none of them consider SOI slot-waveguides with typical geometrical dimensions for CMOS-like production processes using 200 mm SOI wafers with 220 nm high SOH slot-waveguides.
In this work we present to our best knowledge a first comparison of common SOI strip-waveguides with SOI slot-waveguides by the meaning of modal field confinement inside the region of interest.

## 2 SILICON-ON-INSULATOR SLOT-WAVEGUIDES

A SOI slot-waveguide consist of two silicon rails with a fixed height of 220 nm due to common CMOS-like production restrictions. As it can be seen in Figure 1 both silicon rails are located on top of a buried oxide (BOX) substrate and are separated from each other by a slot width $s$ and have a rail width $w$.
Lithographically fabricated slot-waveguides have due to the side-wall roughness relatively high optical losses of 10 dB/cm (Baehr-Jones et al., 2005) which is five times higher compared to common strip-waveguides (Vivien and Pavesi, 2013). Figure 2 shows one scanning electron microscopy picture of three slot-waveguides with different slot widths from the top view and one slot-waveguide in the cross-sectional view recorded with a focused ion beam. They are fabricated in a 130 nm SiGe BiCMOS production line at the Institute of High-Performance Microelectronics (IHP) in Frankfurt (Oder) using 200 mm SOI wafers and 248 nm DUV lithography.

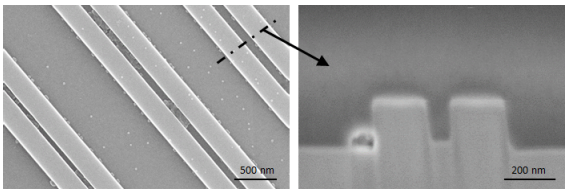

Figure 2: Slot-waveguides with different slot widths fabricated with a 248 nm DUV lithography.

Assuming a wavelength of 1550 nm, the refractive index for the silicon is $n_{si} = 3.48$ and for the BOX substrate $n_{box} = 1.444$ (Palik, 1997; Tsang et al., 2002). The refractive index of the surrounding material $n_{sm}$ is variable because it can be air, gas, fluid or an optical nonlinear material, depending on the application. In the following we will use $n_{clad}$ as cladding refractive index instead of $n_{sm}$ because we will consider an organic cladding material. We choose $n_{clad} = 1.8$ which corresponds to a commercially available and reliable organic material named $M3$ (commercialized by GigOptix Inc.). $M3$ is successfully used for several slot-waveguide based electro-optical modulators like in (Palmer et al., 2013a; Leuthold et al., 2013; Korn et al., 2013; Palmer et al., 2013b).

## 3 SIMULATION OF SLOT-WAVEGUIDES

For the calculation of waveguide eigenmodes we employed a commercial full-vectorial 2D finite element method (FEM) based mode solver from COMSOL Multiphysics®. Doing this we swept several parameters like the silicon rail width and slot width whereas the height is fixed to 220 nm and the wavelength is assumed to be 1550 nm. Triangular vector-elements with a maximum and minimum element size of 8 nm and 6 nm, respectively, have been adopted for meshing the profile. We have always used over $12 \cdot 10^3$ mesh elements. For our simulations we consider a total domain of $D_{tot} = 3\ \mu\text{m}^2$ which is illustrated in Figure 1.
In order to yield the mode field distribution and effective refractive index, the refractive index distribution $n(x,y)$ for the structure shown in Figure 1 need to be declared to calculate eigenvalues and eigenfunctions of the wave equation

$$\nabla \times (\nabla \times \mathbf{E}) - k_0^2 n^2 \mathbf{E} = 0, \qquad (1)$$

where $k_0$ is the wave number in free space. By doing this we get the optical field distribution for the quasi-TE and quasi-TM mode as shown in Figure 3. In the following we will neglect the quasi-TM mode because it is over two times of magnitude smaller than

the quasi-TE mode. However, it should be mentioned that the cross-section capture area for the surface is typically greater for the quasi-TM mode in biosensing applications due to the difficulty in functionalising the interior of the slot.

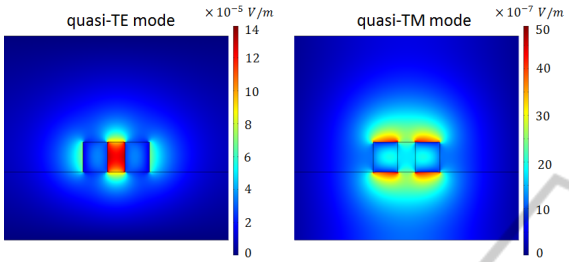


Figure 3: Optical field distribution for the quasi-TE and quasi-TM mode of a SOI slot-waveguide.

## 3.1 Field Confinement Factor of Slot-waveguides

In order to design, develop and improve slot-waveguides for applications in the field of biophotonic or high-speed modulators it is necessary to calculate characteristic values which describe the confinement and therefore the interaction of light with the surrounding material. One figure of merit of how well the guided modal field is confined in a certain region is the so-called field confinement factor. The field confinement factor is usually defined as the ratio of the time averaged power flow in the domain of interest ($D_{int}$) to the time averaged power flow inside the total domain ($D_{tot}$)

$$\Gamma = \frac{\int\int_{D_{int}} Re\{[\mathbf{E}\times\mathbf{H}^*]\cdot\mathbf{e}_z\}\,\mathrm{d}x\mathrm{d}y}{\int\int_{D_{tot}} Re\{[\mathbf{E}\times\mathbf{H}^*]\cdot\mathbf{e}_z\}\,\mathrm{d}x\mathrm{d}y}. \quad (2)$$

$E$ and $H$ are the electric and magnetic field vectors, respectively, and $e_z$ is the unit vector in $z$ direction (Chuang, 2009). There are three different cases in order to choose the domain of interest. In case of common strip-waveguides the domain of interest is equal to the core region, $D_{int}$=$D_{core}$. In contrast to that, for bio-sensing applications the region of the cover medium is considered to be the domain of interest, $D_{int}$=$D_{cover}$, which is valid for strip- and slot-waveguides as well. Considering slot-waveguides for electro-optical modulators the domain of interest is equal to the slot region, $D_{int}$=$D_{slot}$. All possible domains of interest are illustrated in Figure 4. In case of low-index-contrast waveguides, Equation 2 can be simplified using the linear relationship between the electric and magnetic field for a plane-wave

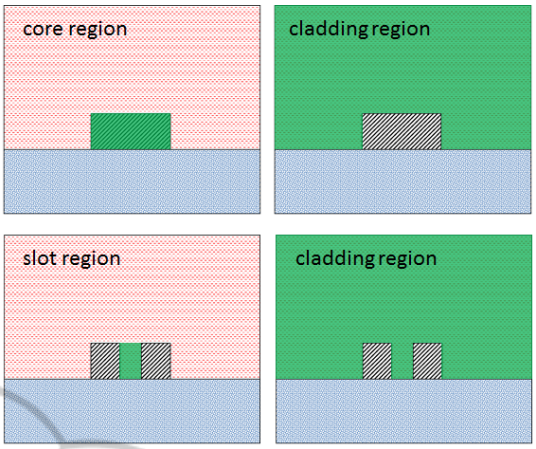


Figure 4: Domains of interest: core $D_{core}$, cladding $D_{clad}$ and slot $D_{slot}$ regions are highlighted in green. Please note that the substrate is not included in the cladding region.

$$\frac{1}{2}\int\int Re\{[\mathbf{E}\times\mathbf{H}^*]\cdot\mathbf{e}_z\}\,\mathrm{d}x\mathrm{d}y = \frac{1}{2}\frac{\beta}{\omega\mu_0}\int\int|\mathbf{E}|^2\,\mathrm{d}x\mathrm{d}y, \quad (3)$$

which leads to

$$\Gamma = \frac{\int\int_{D_{int}}|\mathbf{E}|^2\,\mathrm{d}x\mathrm{d}y}{\int\int_{D_{tot}}|\mathbf{E}|^2\,\mathrm{d}x\mathrm{d}y}. \quad (4)$$

However, for high-index-contrast waveguides and especially for slot-waveguides this linear relationship does not apply since they must satisfy different boundary conditions (Robinson et al., 2008). Consequently, in this work all confinement factors are calculated according to Equation 2.

## 3.2 Effective Nonlinear Area of Slot-waveguides

A figure of merit of how well the waveguide geometry supports the nonlinear interaction is the so called effective nonlinear area (Koos et al., 2007). The smaller the effective nonlinear area provided by the waveguide structure the higher the nonlinear interaction which is important for electro-optical modulators.

For the analysis of low-index-contrast systems, it is usually assumed that the gradient of the dielectric constant is approximately zero in the entire cross section. But this approximation is not valid for high-index-contrast material systems. Therefore, Koos et al. derived the effective nonlinear area for high-index-contrast waveguides in 2007 by using the slowly varying envelope approximation (Koos et al., 2007). The

effective nonlinear area results then from the nonlinear Schrödinger equation

$$A_{eff} = \frac{Z_0^2}{n_{clad}^2} \cdot \frac{\left| \int\int_{D_{tot}} Re\{[\mathbf{E} \times \mathbf{H}^*] \cdot \mathbf{e}_z\} \, dxdy \right|^2}{\int\int_{D_{int}} |\mathbf{E}|^4 \, dxdy}, \quad (5)$$

with the free-space wave impedance $Z_0 = \sqrt{\mu_0/\varepsilon_0} \approx 377\ \Omega$. In our case is the domain of interest equal to the cladding domain, $D_{int} = D_{slot}$. Equation 5 counts for high-index-contrast material systems. In case of low-index-contrast material systems it can be assumed that $n_{core} \approx n_{clad} \approx n_{box} \approx n_{int}$, and the longitudinal field becomes negligible (Koos et al., 2007). Furthermore, the transverse components of the electrical field $E$ and the magnetic field $H$ can be approximated by a scalar function $F$ with the condition $E \approx F \cdot e_x$ and $H \approx (n_{int}/Z_0)F \cdot e_y$ where $e_x$ and $e_y$ are the unit vectors in $x$ and $y$ direction, respectively (Koos et al., 2007). Further it can be stated that $D_{int} = D_{tot}$ if the nonlinearity is homogeneous in $D_{tot}$. Now Equation 5 becomes simplified to

$$A_{eff} = \frac{\left( \int\int_{D_{tot}} |F|^2 \, dxdy \right)^2}{\int\int_{D_{int}} |F|^4 \, dxdy}, \quad (6)$$

which is similar to the common definition of an effective area (Agrawal, 2012).

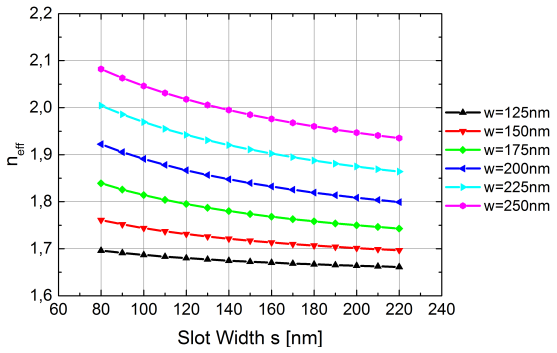


Figure 5: Calculated effective refractive indices $n_{eff}$ of SOI slot-waveguides as function of the slot width $s$ and with the rail width $w$ as parameter.

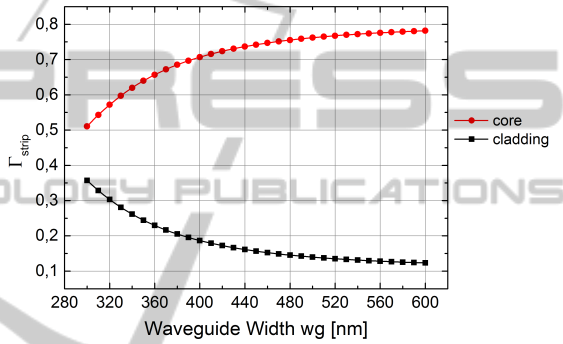


Figure 6: Field confinement factor $\Gamma_{strip}$ of conventional SOI strip-waveguides for the core and cladding region as a function of the waveguide width $wg$.

## 4 RESULTS AND DISCUSSION

Calculated effective refractive indices $n_{eff}$ as a function of the slot width $s$ of SOI slot-waveguides are shown in Figure 5. It can be seen that the effective refractive index becomes higher by increasing the rail width $w$ and by decreasing the slot width $s$.

Figure 6 shows the obtained field confinement factor $\Gamma_{strip}$ for a silicon strip-waveguide. The domains of interest are the core and the cladding. Please note that the substrate is not included in the cladding domain. Therefore, the sum of core and cladding field confinement factor is not equal to unity. As it can be seen there is a high light confinement in the core region. These results are in good agreement with the literature (Vivien and Pavesi, 2013). In order to maximize the sensitivity of SOI slot-waveguide based label-free sensors it is necessary to maximize the field confinement factor of the cladding $\Gamma_{clad}$. From Figure 7 it can be seen that the confinement in the cladding region is increased by decreasing the rail width $w$ and increasing the slot width $s$. For $w = 180$ nm the highest confinement in the cladding region is obtained in the parameter range of our simulation. This result is in good agreement with (Dell'Olio and Passaro, 2007). For the slot-waveguide with $w = 180$ nm and $s = 180$ nm we obtain a field confinement factor of $\Gamma_{clad} = 0.69$. This is an enhancement of about five times compared to a conventional strip-waveguide with a typical waveguide width of $wg = 500$ nm. With that result, the high sensitivity of slot-waveguide based label-free sensors as stated by Claes et al. can be explained (Claes et al., 2009). However, due to the difficulty in functionalising the interior of the slot the sensitivity can be smaller than expected.

In order to improve SOI slot-waveguides for electro-optical applications it is necessary to find the highest confinement in the slot region. Figure 8 depicts the obtained field confinement factors for the slot region $\Gamma_{slot}$ as a function of the slot width $s$ and the rail width $w$ as parameter. It can be seen that there is one maximum of the highest field confinement of $\Gamma_{slot} = 0.216$ at a slot width of $s = 116$ nm and a rail width of $w = 200$ nm. This is about four times smaller compared to a SOI strip-waveguide. However, in this case it is more convenient to relate the field confinement factor $\Gamma_{slot}$ to the area where the

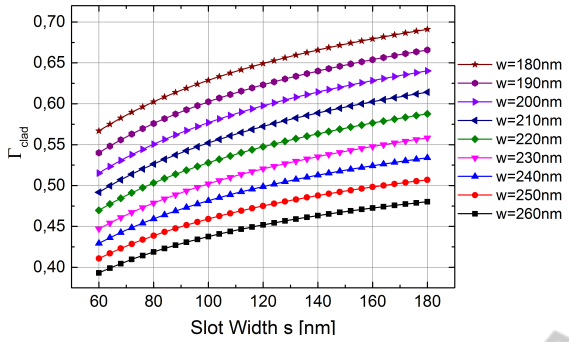


Figure 7: Field confinement factor $\Gamma_{clad}$ of a SOI slot-waveguide for the cladding region in dependence on the slot width $s$.

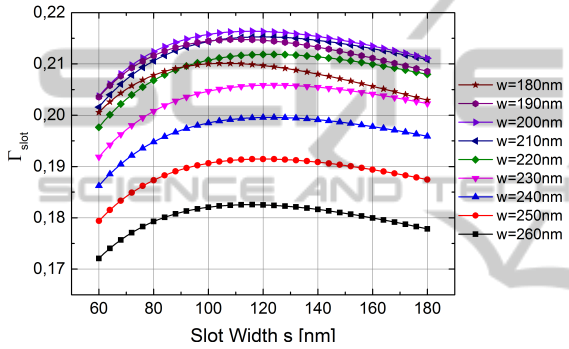


Figure 8: Field confinement factor $\Gamma_{slot}$ of a SOI slot-waveguide for the slot region as a function of the slot width $s$ and the rail width $w$ as parameter.

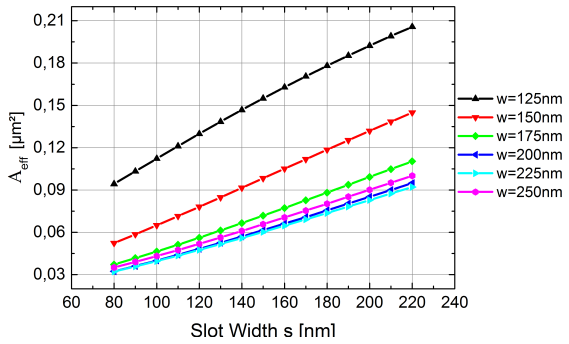


Figure 9: Calculated effective nonlinear area $A_{eff}$ of SOI slot-waveguides in dependence on the slot width $s$. The rail width $w$ was varied as parameter.

light is confined as figure of merit, $FOM = \Gamma_{slot}/A_{slot}$ and $FOM = \Gamma_{strip}/A_{strip}$. In our case $A_{slot}$ is equal to $D_{slot}$ and $A_{strip}$ is equal to $D_{core}$. With that we can show for our example that the FOM for a SOI slot-waveguide ($s = 116$ nm, $w = 200$ nm) is about four times higher compared to that one of a strip-waveguide ($wg = 500$ nm) which confirms our results for the cladding field confinement and other publications like (Almeida et al., 2004).

Furthermore, it is necessary to minimize the effective nonlinear area $A_{eff}$ in order to improve SOI slot-waveguides for third order nonlinear effects. Figure 9 indicates that there is a minimum in the parameter range of our simulation of $A_{eff} = 0.032\ \mu m^2$ for a slot width of $s = 80$ nm and a rail width of $w = 225$ nm. Our results are in good agreement with (Muellner et al., 2009).

## 5 CONCLUSION

Simulation and analysis of SOI slot-waveguides have been carried out and field confinement factors and effective nonlinear areas have been thoroughly calculated with the Finite Element Method. Field confinement factors have been calculated in the slot and cladding region. According to our simulation, SOI slot-waveguides provide about five times higher field confinement in the cladding region compared to conventional SOI strip-waveguides. These results can be used for design optimization in order to achieve optimal SOI slot-waveguide dimensions for sensing applications. For the slot region we have found a maximum confinement of $\Gamma_{slot} = 0.216$ which is compared to a SOI strip-waveguide about four times smaller. However, relating it to the area there the light is confined it is four times higher compared to a SOI strip-waveguide. For the effective nonlinear area we have found a minimum of about $A_{eff} = 0.032\ \mu m^2$ for our simulated parameter range. In total, we have demonstrated design trade-offs and an approach in order to improve SOI slot-waveguide structures.

## ACKNOWLEDGEMENTS

The authors would like to thank the German Federal Ministry of Education and Research (BMBF) for the financial support under contract no. 03FH086PX2, the University of Applied Sciences Wildau (THWi), Germany, and the Ministry of Science, Technology and Culture of the federal state Brandenburg, Germany, for financial support. The authors would also like to thank Fr. Nanni, P. Prosposito, F. De Matteis, and R. De Angelis from the University of Rome Tor Vergata, Italy, St. Meister and A. Al-Saadi from the Technical University Berlin, Germany, and L. Zimmermann, D. Knoll, D. Stolarek, J. Katzer, St. Lischke, H. Silz, B. Tillack and W. Mehr from the Institute of High-Performance Microelectronics (IHP), Germany, for their encouragement and support in the framework of the Joint-Lab IHP-THWi.

## REFERENCES


Agrawal, G. (2012). *Nonlinear Fiber Optics*. Academic Press, 5 edition.

Almeida, V. R., Xu, Q., Barrios, C. A., and Lipson, M. (2004). Guiding and confining light in void nanostructure. *Opt. Lett.*, 29(11):1209–1211.

Baehr-Jones, T., Hochberg, M., Walker, C., and Scherer, A. (2005). High-q optical resonators in silicon-on-insulator-based slot waveguides. *Applied Physics Letters*, 86(8):081101.

Barrios, C. A., Gylfason, K. B., Sánchez, B., Griol, A., Sohlström, H., Holgado, M., and Casquel, R. (2007). Slot-waveguide biochemical sensor. *Opt. Lett.*, 32(21):3080–3082.

Chuang, S. L. (2009). *Physics of Photonic Devices*. Wiley, 2 edition.

Claes, T., Molera, J., De Vos, K., Schachtb, E., Baets, R., and Bienstman, P. (2009). Label-free biosensing with a slot-waveguide-based ring resonator in silicon on insulator. *Photonics Journal, IEEE*, 1(3):197–204.

Dell'Olio, F. and Passaro, V. M. (2007). Optical sensing by optimized silicon slot waveguides. *Opt. Express*, 15(8):4977–4993.

Feng, N.-N., Michel, J., and Kimerling, L. (2006). Optical field concentration in low-index waveguides. *Quantum Electronics, IEEE Journal of*, 42(9):885–890.

Koos, C., Jacome, L., Poulton, C., Leuthold, J., and Freude, W. (2007). Nonlinear silicon-on-insulator waveguides for all-optical signal processing. *Opt. Express*, 15(10):5976–5990.

Korn, D., Palmer, R., Yu, H., Schindler, P. C., Alloatti, L., Baier, M., Schmogrow, R., Bogaerts, W., Selvaraja, S. K., Lepage, G., Pantouvaki, M., Wouters, J. M., Verheyen, P., Campenhout, J. V., Chen, B., Baets, R., Absil, P., Dinu, R., Koos, C., Freude, W., and Leuthold, J. (2013). Silicon-organic hybrid (soh) iq modulator using the linear electro-optic effect for transmitting 16qam at 112 gbit/s. *Opt. Express*, 21(11):13219–13227.

Leuthold, J., Koos, C., Freude, W., Alloatti, L., Palmer, R., Korn, D., Pfeifle, J., Lauermann, M., Dinu, R., Wehrli, S., et al. (2013). Silicon-organic hybrid electro-optical devices. *Selected Topics in Quantum Electronics, IEEE Journal of*, 19(6):3401413–3401413.

Muellner, P., Wellenzohn, M., and Hainberger, R. (2009). Nonlinearity of optimized silicon photonic slot waveguides. *Opt. Express*, 17(11):9282–9287.

Palik, E. D. (1997). *Handbook of Optical Constants of Solids*. Academic Press, 1 edition.

Palmer, R., Alloatti, L., Korn, D., Schindler, P., Baier, M., Bolten, J., Wahlbrink, T., Waldow, M., Dinu, R., Freude, W., Koos, C., and Leuthold, J. (2013a). Low power mach-zehnder modulator in silicon-organic hybrid technology. *Photonics Technology Letters, IEEE*, 25(13):1226–1229.

Palmer, R., Alloatti, L., Korn, D., Schindler, P., Schmogrow, R., Heni, W., Koenig, S., Bolten, J., Wahlbrink, T., Waldow, M., Yu, H., Bogaerts, W., Verheyen, P., Lepage, G., Pantouvaki, M., Van Campenhout, J., Absil, P., Dinu, R., Freude, W., Koos, C., and Leuthold, J. (2013b). Silicon-organic hybrid mzi modulator generating ook, bpsk and 8-ask signals for up to 84 gbit/s. *Photonics Journal, IEEE*, 5(2):6600907–6600907.

Robinson, J. T., Preston, K., Painter, O., and Lipson, M. (2008). First-principle derivation of gain in high-index-contrast waveguides. *Opt. Express*, 16(21):16659–16669.

Tsang, H., Wong, C., Liang, T., Day, I., Roberts, S., Harpin, A., Drake, J., and Asghari, M. (2002). Optical dispersion, two-photon absorption and self-phase modulation in silicon waveguides at 1.5 $\mu$m wavelength. *Applied Physics Letters*, 80(3):416–418.

Vivien, L. and Pavesi, L., editors (2013). *Handbook of Silicon Photonics*. CRC Press, 0 edition.

Weimann, C., Schindler, P. C., Palmer, R., Wolf, S., Bekele, D., Korn, D., Pfeifle, J., Koeber, S., Schmogrow, R., Alloatti, L., Elder, D., Yu, H., Bogaerts, W., Dalton, L. R., Freude, W., Leuthold, J., and Koos, C. (2014). Silicon-organic hybrid (soh) frequency comb sources for terabit/s data transmission. *Opt. Express*, 22(3):3629–3637.